



Research



Cite this article: Brantut N. 2025 Semi-brittle flow of rocks: cracks, dislocations and strain hardening. *Proc. R. Soc. A* **481**: 20240189. <https://doi.org/10.1098/rspa.2024.0189>

Received: 12 March 2024

Accepted: 5 December 2024

Subject Category:

Earth science

Subject Areas:

geophysics, geology, materials science

Keywords:

semi-brittle, hardening, dislocation, fracture

Author for correspondence:

Nicolas Brantut

e-mail: nicolas.brantut@gfz.de

Semi-brittle flow of rocks: cracks, dislocations and strain hardening

Nicolas Brantut^{1,2}

¹Department of Earth Sciences, University College London, London, UK

²GFZ Helmholtz Centre for Geosciences, Potsdam, Germany

NB, 0000-0002-1704-7468

Strain hardening is a key feature observed in many rocks deformed in the so-called ‘semi-brittle’ regime, where both crystal plastic and brittle deformation mechanisms operate. Dislocation storage has long been recognized as a major process leading to strain hardening. Here, it is suggested that tensile microcracks may be viewed as dislocation sinks, by offering internal free surfaces where dislocations can escape individual crystals within an aggregate. Strain hardening is modelled with a conventional approach, combining Taylor’s equation relating stress to dislocation density, and a dislocation density evolution law based on dislocation mean-free path and dynamic recovery. The initiation of microcracks is modelled as a function dislocation density, assuming dislocation pile-ups at grain boundaries. Microcrack growth is modelled using linear elastic fracture mechanics. The model captures important qualitative features observed in calcite marble deformation experiments: pressure-dependency of strength in the ductile regime and a reduction in hardening linked to an increase in crack growth with decreasing confining pressure. Grain size dependency of strength and hardening is also captured but requires significant toughening (or limitation to crack growth) at small grain sizes. The model can be improved significantly once detailed, systematic microstructural observations become available.

1. Introduction

With increasing pressure and temperature, rocks transition from a brittle behaviour marked by

© 2025 The Author(s). Published by the Royal Society under the terms of the Creative Commons Attribution License <http://creativecommons.org/licenses/by/4.0/>, which permits unrestricted use, provided the original author and source are credited.

microcracking that leads to macroscopic failure, to a fully plastic behaviour where deformation can be accommodated in a distributed fashion by crystal plastic processes such as dislocation motion and solid-state diffusion (e.g. [1]). In the transitional regime, at pressures sufficiently high to suppress macroscopic faulting, and temperatures sufficiently low to limit diffusion, most rocks behave in a semi-brittle, ductile fashion (e.g. [1–3]). Deformation is accommodated by a combination of microscopic slip at interfaces (shear cracks), tensile microcracks, and crystal plastic processes such as twinning and dislocation motion. This behaviour is well documented in rocks like calcite marble [4,5], quartzite [6] and peridotite [7].

Strain hardening is a key feature of ductile rock deformation in the semi-brittle regime: under typical laboratory conditions and sample sizes, flow stress does not reach a clear steady-state (e.g. [5]), which implies that microstructures keep evolving (as evidenced, for instance, by acoustic emission signals [8]). Strain hardening is now recognized to be an important phenomenon that controls the strength of the lithosphere (e.g. [9–11]), but its physical underpinning is not fully understood.

In general, strain hardening is produced by microstructural changes that either increase the internal elastic stress in the material or raise the critical stress required to drive the motion of carriers of deformation (e.g. [12,13]). In the semi-brittle regime of rocks, two main hardening mechanisms can be distinguished: (i) increase in elastic restoring forces (sometimes also called backstresses) due to slip across pre-existing defects (e.g. cracks) in an otherwise elastic matrix (e.g. [14,15]) and (ii) increase in strength due to accumulation of stored dislocations in deforming crystals (e.g. [16]). Slip across pre-existing defects (in an otherwise elastic matrix) is a general process and is not restricted to dislocation glide: frictional slip is also a potentially important phenomenon at low temperature and low pressure in many rock types (e.g. [15,17,18]). Twinning can also produce backstress (e.g. [19]).

In the semi-brittle regime, the role of tensile microcracks on strength is not clear. Microcracks do not strongly interact to produce a localized macroscopic shear fault, but they produce significant dilation (e.g. [4,20]). In addition, there is an inverse dependency between the degree of microcracking and the hardening rate; experiments in calcite marble have shown that higher crack densities are associated with lower hardening rates [4,21]. This correlation is observed mainly as a function of confining pressure: low confining pressures promote higher crack densities, lower strength and lower hardening rates. By contrast, at elevated confining pressure, the differential stress is larger, lower crack densities and more intracrystalline defects are observed [4,22]. Only a few micromechanical models have been developed where tensile crack growth is coupled to plastic flow. The early approach of Horii & Nemat-Nasser [23] was based on an extension of the ‘wing crack’ model (originally developed to understand crack growth in brittle solids) and included shear flaw extension into plastic zones. Recent re-examination of this model [17] showed that this approach leads to useful insights into the onset of microcracking in the semi-brittle regime but does not appropriately reproduce the full stress–strain behaviour. Similarly, the model of Renshaw & Schulson [24] introduces plastic relaxation near crack tips in an otherwise brittle model, which is useful to make predictions of fracture strength, but not to stress–strain behaviour. By contrast, Nicolas *et al.* [25] presented a coupled model, including crack growth and dislocation glide, aimed to predict stress–strain behaviour, dilatancy, compaction and crack density evolution during high pressure deformation of porous limestone. While quite successful, the model of Nicolas *et al.* [25] is made very complex due to the need to account for frictional processes and void enlargement/compaction in addition to plastic flow and tensile cracking.

A full account of the coupling between dislocation accumulation, microcrack growth and possibly other effects such as twinning should eventually be produced by dislocation dynamics simulations informed by well-defined material constants (e.g. [26]). In the context of rock forming minerals, this task is simply beyond our current capabilities, and it is useful to consider more phenomenological alternatives to explore, at least semi-quantitatively, the possible role of microcracks on plastic flow of rocks.

The goal of this note is to develop a simple model to explain how microcracking may be coupled to dislocation glide to produce some of the weakening effect observed in experiments. Our starting point will be the ‘one state variable’ flow law of Mecking & Kocks [12] and Estrin & Mecking [27], where dislocation density determines the full evolution of stress–strain behaviour. This model, which we will refer to as the ‘Kocks–Mecking–Estrin’ (abbreviated KME) model, has proved very successful to understand the behaviour of many metals (see review by [13]). It has also been extended to include the role of twins in metals (e.g. [28,29]), which may also apply to rock-forming minerals [5,21]. Here, we propose to include the effect of microcracks on dislocation density evolution by considering that open cracks act as dislocation sinks, so that an increased crack density leads to a decrease in strain hardening, as observed experimentally. The nucleation and growth of tensile cracks will be coupled to dislocation density evolution by considering that cracks nucleate from dislocation pile-ups, an approach that was used by Nicolas *et al.* [25]. Other sources of microcracking (related to other types of microstructural defects) could be introduced in the same framework and will be discussed. While much experimental work is still needed to confirm the validity of the approach, the present work provides a first quantitative attempt to explain some key aspects of semi-brittle flow in rocks, and testable predictions are suggested.

2. Model

(a) Dislocation-based strain hardening process

The KME model is based on the Taylor relationship [16] relating the resolved shear stress τ on a particular slip plane to dislocation density ρ as

$$\tau = \tau_0 + \alpha b G \sqrt{\rho}, \quad (2.1)$$

where τ_0 is a constant minimal stress required to move dislocation (lattice friction), α is a constant of $O(1)$ that represents the dislocation interactions leading to hardening, b is the magnitude of the Burgers vector representative of the characteristic slip system producing hardening and G is the shear modulus. For polycrystalline aggregates under differential stress conditions, (2.1) can be generalized to

$$\sigma = \sigma_0 + M \alpha' b G \sqrt{\rho}, \quad (2.2)$$

where σ_0 is a yield stress for the aggregate (typically, thermally activated), M is a geometrical factor related to activation of multiple slip systems in different orientations (sometimes called ‘Taylor’ factor) and α' is the modified α value that accounts for the geometry of loading (i.e. the relation between applied stress and resolved shear stress). For triaxial loading conditions, we have $\alpha' = 2\alpha$. The term $M \alpha' b G \sqrt{\rho}$ corresponds to a ‘backstress’, i.e. the additional stress required to move dislocations, which arises from dislocation interactions (e.g. dislocation tangles).

The relationship (2.1) is well established both experimentally and theoretically in face-centred cubic (FCC) metals, and α has been shown to be close or equal to 0.4 (e.g. [30]). In rock-forming minerals, Taylor’s relation should also apply, but the relative importance of the backstress terms with respect to other terms (lattice friction) is difficult to determine. In the low temperature regime, experimental data for quartz [31], calcite [32], plagioclase and olivine [33] all show that (2.1) is reasonably accurate, with α ranging from 1 to 1.5. It is also observed experimentally in polycrystalline aggregates, at least at relatively high stress [32]. In olivine, recent work by Breithaupt *et al.* [34] has shown that the Taylor relationship (2.2) is applicable provided that the τ_0 (or, equivalently σ_0) term is properly accounted for, which was not necessarily recognized in previous studies [35–37]. In most rock-forming minerals, the experimentally inferred α is of the order of 1 or more, which is high compared with that in fcc metals (0.4). This difference might arise from observational bias in the presence of a high lattice

friction (e.g. [38]), but could also originate from stronger dislocation interactions in crystals with low symmetries. Regardless of this debate, Taylor's equation includes a fundamental effect that explains, at a set of fixed conditions, how dislocation accumulation can lead to strain hardening.

The Taylor equation (2.2) includes the average effect of dislocations on the stress required to deform the material. There might be other contributions in the form of backstress, i.e. elastic restoring forces appearing due to distortion of crystals during deformation, that can be accounted for by modifying equation (2.2) as follows (e.g. [39]):

$$\sigma = \sigma_0 + M\alpha' bG\sqrt{\rho} + \sigma_b, \quad (2.3)$$

where σ_b denotes the additional backstress that could arise from other mechanisms or specific dislocation configurations. Experimental evidence for the existence of backstress is in the form of the Bauschinger effect, where material yields at a different threshold during reversal of deformation direction: the backstress 'helps' yielding during strain reversal because it acts as a reaction force that opposes the initial loading direction.¹ Such an effect has been observed in olivine ([9,33,41]) and may be relevant in other rock-forming minerals.

Here, we follow Sinclair *et al.* [39] and consider that backstress arises from dislocation pile-ups at obstacles such as grain boundaries. For an isolated dislocation pile-up of length L containing n_p dislocations of Burgers vector b , elastic equilibrium requires that the driving stress (here equivalent to our backstress) is [42]

$$\sigma_b = \frac{G}{\pi(1-\nu)} \frac{n_p b}{L}, \quad (2.4)$$

where ν is Poisson's ratio. In general, equation (2.4) should represent an upper bound for the net, average backstress in a polycrystalline aggregate: while the expression applies locally to an isolated dislocation pile-up, the net effect on the average stress at aggregate level may be much smaller due to interactions and superposition of pile-ups of different signs and orientations.

The number of dislocations in pile-ups, n_p , is expected to be connected to the total number of dislocations in the material, represented by the dislocation density ρ . In a hardening model including backstress from dislocation pile-ups, Sinclair *et al.* [39] suggested an evolution law for n_p such that n_p saturates at some characteristic upper bound, which is meant to represent the relaxation of elastic stress concentrations due to stabilization of pile-ups by dislocations of opposite signs.

Here, in the absence of detailed observations in rock-forming minerals, an alternative, simpler approach is proposed. Any additional backstress σ_b can only exist if (i) there are sufficiently 'opaque' barriers to dislocation motion and (ii) there is an imbalance in net dislocation signs across barriers. It is possible to accumulate (store) dislocations without generating significant backstress, as long as the stored dislocations are in a stable configuration: therefore, only a fraction of the total dislocation density is expected to be present in 'unbalanced' pile-ups. If we denote this fraction ϕ , we can then write the number of dislocations in each pile-up as

$$n_p = \phi\rho/\rho_{pu}, \quad (2.5)$$

where ρ_{pu} is the pile-up density (defined as in Nicolas *et al.* [25], $\rho_{pu} = 1/L_{pu}^2$ where L_{pu} is the spacing between pile-ups).

The total dislocation density ρ is the internal state variable that determines the stress evolution during deformation. Based on extensive experimental observations in metals deformed at low temperature, the evolution of ρ with plastic strain has been found to be well captured by a relation of the form (e.g. [13])

$$\frac{d\rho}{d\varepsilon} = \frac{1}{b\lambda} - f\rho - R(T, \dot{\varepsilon}, \dots), \quad (2.6)$$

¹This effect is the analogue of the stress-memory effect due to frictional slip in brittle rocks (e.g. [18,40]).

where ϵ is the shear strain, λ is the dislocation mean-free path, f is a dynamic recovery parameter (that depends weakly on temperature and strain rate), and R is a collective term denoting other potential recovery processes (e.g. [34,43]). Equation (2.6) is written in terms of strain increments, following the requirement that dislocation nucleation is due to imposed deformation. A more general approach, detailed in Breithaupt [43], would involve an evolution law for ρ with increments of time, which is a more natural independent variable when considering static recovery processes and rate-dependent dislocation creep. Here, we use the form (2.6) because we focus on the strain-hardening behaviour of rocks at low temperatures, where rate effects are minor (e.g. [5]).

The dislocation mean-free path is impacted by two major obstacles: grain boundaries and other dislocations (figure 1a). A common form for λ is

$$1/\lambda = 1/d + k\sqrt{\rho}, \quad (2.7)$$

where d is the grain size and k is a constant. The term $k\sqrt{\rho}$ describes so-called ‘forest hardening’, i.e. the potential for existing dislocations to ‘pin’ the motion of other dislocations and produce tangles.

The combination of equations (2.2), (2.6) and (2.7) has been very effective in understanding the strain-hardening behaviour in many materials where dislocations are the main carrier of deformation [13]. What is proposed here is an extension of this approach where the existence of cracks is accounted for.

(b) Crack nucleation and growth

In crystals where dislocation glide is active but not on sufficiently many slip systems to produce fully plastic flow, dislocations may pile up at obstacles and raise internal stress, which leads to microcracking (figure 1a). Cracking associated with dislocation glide has been studied by Stroh ([46,47], among others). The effect of pressure on crack nucleation during plastic flow was established by Francois & Wilshaw [48] and studied more systematically by Wong [45]. The model of Wong [45] was used recently in the semi-brittle micromechanical model of Nicolas *et al.* [25].

As a note of caution, it should be stated that direct experimental support for microcracking due to dislocation pile-up remains at best incomplete in geological materials. Potential observations have been discussed in the original work of Wong [45]. Cracks are often spatially associated with dislocations in rocks deformed in the semi-brittle regime [4,7,49,50], but it is not clear whether cracking is induced by dislocations. Despite the uncertainty of the fracturing mechanism, cracks are observed to interact with dislocations in many instances (e.g. [4]), and in the absence of solid alternative processes we will follow Nicolas *et al.* [25] and work on the hypothesis that dislocation pile-ups are one of the main potential sources of microcracks in the semi-brittle regime.

The condition for crack nucleation ahead of a pile-up is given by [45]

$$K_{Ic} = \frac{4\sqrt{2}}{\sqrt{3\pi}} \tau_{\text{eff}} \sqrt{L}, \quad (2.8)$$

where K_{Ic} is the fracture toughness, L is the length of the pile-up (that should be commensurate to the grain size, or, to the dislocation mean-free path), and τ_{eff} is the stress driving the dislocations in the pile-up. The number of dislocations in the pile-up is given by

$$n_p = \frac{\pi(1-\nu)L\tau_{\text{eff}}}{bG}, \quad (2.9)$$

so the nucleation condition is satisfied if [25]

$$n_p > n_c = \frac{\pi\sqrt{3\pi L}}{8bG/(1-\nu)} K_{Ic}. \quad (2.10)$$

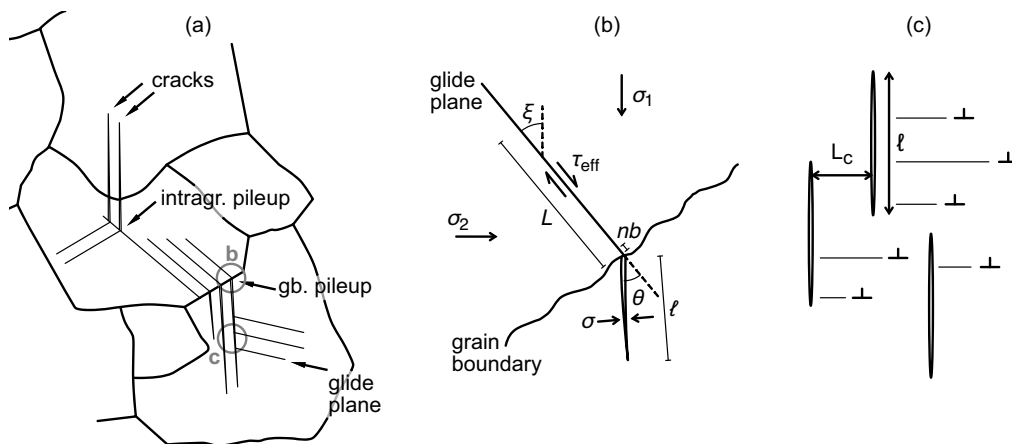


Figure 1. (a) Schematic of the key microstructural elements captured by the model. Dislocation motion along slip planes produces pile-ups (with density ρ_{pu}) at grain boundaries or inside grains (due to other dislocations or twins that could act as obstacles). Some pile-ups produce tensile microcracks. The microcracks act as free surfaces where dislocations are absorbed. (b) Schematic of a crack nucleated at a pile-up. Modified from Olsson *et al.* [44] and Wong [45]. (c) Schematic of the dislocation absorption mechanism: dislocations move and may encounter cracks (free surfaces) of length ℓ , with an average spacing of L_c .

Once a crack is nucleated at a pile-up, it will grow to maintain the condition $K_I \leq K_{Ic}$. The mode I stress intensity factor at the tip of the open crack is given by [45]

$$K_I = n_p b \frac{G}{1-\nu} \frac{\sin \theta}{\sqrt{2\pi\ell}} - \sigma_n \sqrt{\pi\ell/2}, \quad (2.11)$$

where θ is the angle between the pile-up plane and the open crack, ℓ is the open crack length and σ is the normal stress applied on the open crack (positive in compression), expressed as (see notations and geometry in figure 1b)

$$\sigma_n = \frac{\sigma_1 + \sigma_2}{2} - \frac{\sigma_1 - \sigma_2}{2} \cos(2(\theta - \xi)). \quad (2.12)$$

(c) Feedback between cracking and dislocation storage

If $n_p > n_c$, cracks will nucleate at pile-ups. How would this impact strength? Open microcracks tend to reduce the effective elastic moduli of the material at the macroscopic scale (e.g. [51,52]), which leads to enhanced compliance, but this effect has no impact on the flow stress (the shear modulus G relevant to Taylor's equation is the one at lattice scale). One may think that cracking would relax the backstress. This is true locally at the head of the pile-up, but tensile cracking does not suppress elastic stresses: it merely displaces the stress concentration from the original pile-up front to the tensile crack front. There is always an elastic restoring force associated with the slip accumulated along the pile-up plane (see analogous case of the wing crack, e.g. [52]). The backstress could be reduced if the tensile crack tip is shielded by plastic deformation, e.g. by a cloud of dislocations ([53], §7.3).

The open microcracks provide free surfaces inside the material. Free surfaces act as dislocation sinks ([54], Chap. 9): mobile dislocations reaching free surfaces generate steps, and the dislocation line disappears from the crystal. The dislocation density change due to the presence of free surfaces can be written ([54], Equation 9.6)

$$\left(\frac{d\rho}{d\varepsilon}\right)_{\text{free}} = -\frac{1}{b\lambda_c}, \quad (2.13)$$

where λ_c is the characteristic spacing between cracks along the dislocation glide plane (see schematic in figure 1c). Considering an array of parallel cracks of length ℓ spaced on average by the distance L_c , we can estimate the mean distance for a dislocation gliding perpendicular to the cracks to reach a crack plane by

$$\lambda_c = L_c^3/\ell^2. \quad (2.14)$$

We can verify that $\lambda_c \rightarrow \infty$ for $\ell \rightarrow 0$ (i.e. dislocations never reach a crack surface if there are no cracks), and $\lambda_c = L_c$ for $\ell = L_c$ (i.e. dislocations travel an average distance L_c to reach a crack surface if the crack length is equal to the crack spacing).

Including the contribution (2.13) in the dislocation evolution model, we obtain

$$\frac{d\rho}{d\varepsilon} = \frac{1}{b} \left(\frac{1}{d} - \frac{\ell^2}{L_c^3} + k\sqrt{\rho} \right) - f\rho - R(T, \dot{\varepsilon}, \dots), \quad (2.15)$$

where we see how crack growth might lead to a reduction in dislocation storage rate and therefore in hardening rate.

(d) A remark on twinning

The model as derived above only includes the effect of dislocations and microcracks on strength and hardening. We would like to test the model predictions and compare them with experimental data on rocks. The rock type that has been most extensively studied in the semi-brittle regime is calcite marble (more specifically, Carrara marble): this material is known to easily twin during deformation (e.g. [22,55,56], among many others), and twinning has been suggested to contribute significantly to strain hardening [5] and strain distribution in polycrystals [56,57]. In this section, we discuss an extension of the model that includes the role of twins. This is however not an essential element of the analysis that aims to focus on the role of cracks, and this is only provided for completeness and an improved quantitative analysis of data obtained on calcite.

The KME model has been successfully extended to account for the presence of twins (e.g. [28]). One key feature of the stress–strain behaviour of metals that produces twins during deformation is the large hardening rate, orders of magnitude larger than those typical in metals [29]. This behaviour may be explained by the fact that twin boundaries are obstacles to dislocation motion, and thus considerably reduce the dislocation mean-free path λ . This effect can be accounted for by expressing (e.g. [28])

$$1/\lambda = 1/d + 1/t + k\sqrt{\rho}, \quad (2.16)$$

where t is the twin spacing. While an expression like (2.16) has been very successful in explaining the behaviour of twinning-induced plasticity in steel, its validity has not yet been thoroughly tested in rocks such as calcite (which has an easy twin system active at low temperature). Recent experimental data on calcite marble by Rybacki *et al.* [5] suggest that the approach remains valid, but Harbord *et al.* [21] have obtained results that indicate that the effect of grain size might be dominant over the effect of twin density in controlling hardening rate. The relatively minor role of twinning compared with that of grain size might be explained by the ease of slip transmission across twin boundaries in calcite [21]. In general, we expect different types of obstacles to contribute differently to the dislocation mean-free path, depending on their effectiveness in stopping dislocations. We could thus write

$$1/\lambda = k_d/d + k_t/t + k\sqrt{\rho}, \quad (2.17)$$

where k_d and k_t are weighting factors that reflect the ‘opacity’ of each barrier type. These coefficients are phenomenological in nature, but should be correlated to slip transmission coefficients across grain and twin boundaries, respectively (e.g. [21,58]). In practice, there

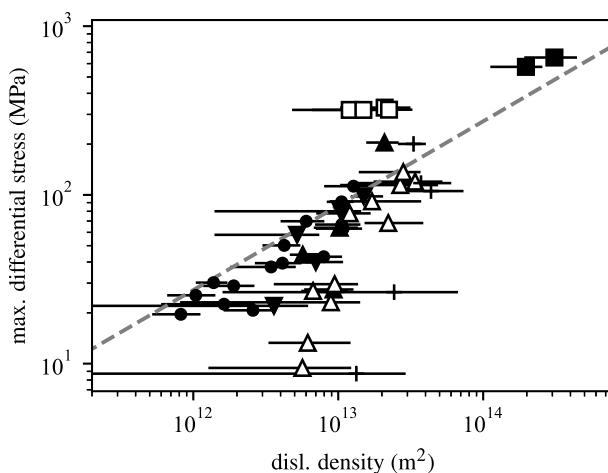


Figure 2. Stress vs. dislocation density in calcite, as compiled and corrected originally by de Bresser [32]. Dashed line is (2.2) with constant modulus $G = 32$ GPa, $b = 6.37$ and $M\alpha' = 1.34$. Symbols are: • single crystals deformed at $T \geq 550^\circ\text{C}$ (de Bresser, 1996); □ Carrara marble deformed at room temperature and P_c ranging from 120 to 300 MPa [4]; ▲ Carrara marble deformed at $P_c = 300$ MPa and temperatures from 600 to 1000°C [32]; ▼ Yule marble deformed at 500 MPa and 600 to 800°C [60]; ■ Solnhofen limestone deformed at room temperature and $P_c = 200$ to 220 MPa [61]; △ Carrara marble deformed at 300 MPa and 600 to 1050°C [62]; + Solnhofen limestone deformed at 300 MPa and 600 to 900°C [63].

are currently insufficient experimental constraints to warrant a detailed breakdown of such empirical constants, and grain size and twin density effects can be lumped into a single ‘effective’ quantity d_{eff} such that

$$1/d_{\text{eff}} = k_d/d + k_t/t. \quad (2.18)$$

Furthermore, in the case of calcite, d_{eff} can be approximated as a constant, since twin density is only weakly dependent on strain in this material [22,59].

3. Parameters and unknowns

The model contains a number of parameters that need to be constrained experimentally. This is a challenging task because only a few datasets exist that relate stress, strain and dislocation density together with semi-brittle flow in rocks. The prime candidate is calcite marble, where the most complete dataset exists in the regime of interest.

For calcite single crystals as well as polycrystals at high stress and high temperature ($> 550^\circ\text{C}$), the Taylor relationship (2.2) adequately fits in the high stress regime (figure 2), with parameters $M\alpha' = 1.34$, $b = 6.37$, and an average shear modulus $G = 32$ GPa [32]. The good fit with most polycrystalline aggregates also implies that specific backstress due to pile-ups plays a minimal role and could potentially be neglected. Note that dislocation densities measured in samples deformed at room temperature [4] do not strictly follow the trend of single crystals, with stress higher than expected for the rather moderate observed dislocation densities. It is possible that the additional stress at a given dislocation density arises from backstress due to dislocation pile-ups or twins, or from frictional processes that could still be significant at the low pressure (around 100 MPa) used in Fredrich *et al.* [4] experiments. A discussion of the behaviour at low stress, not directly relevant to our model of semi-brittle flow, can be found in de Bresser [32].

If we consider single crystals, thus neglecting grain size effects, it is possible to estimate parameters k and f from the data compiled in de Bresser [32] (figure 3). Neglecting size effects ($d \gg 1$) and assuming no additional static recovery effects, the solution of (2.6) is

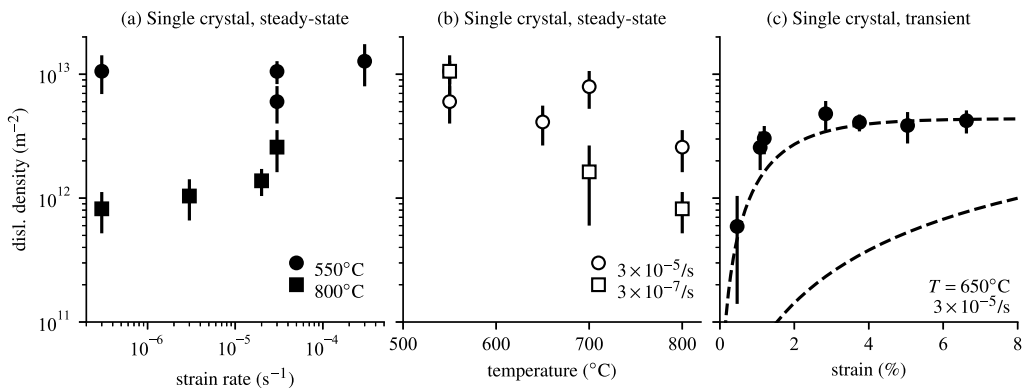


Figure 3. Dislocation density in calcite single crystals as measured by de Bresser [32]. Plots (a) and (b) are steady-state data at different temperatures and strain rates, and plot (c) shows variations in dislocation density as a function of strain. Dashed line in (c) is a fit to (3.1) with $k = 0.2$, $f = 150$ and $\rho_0 = 10^{10} \text{ m}^{-2}$.

$$\rho(\epsilon) = \left[e^{-f\epsilon/2} (\sqrt{\rho_0} - k/(bf)) + k/(bf) \right]^2, \quad (3.1)$$

where ρ_0 is the initial dislocation density. The steady-state dislocation density is $\rho_{\text{ss}} = (k/(bf))^2$. Both steady-state and transient dislocation density measurements (figure 3) can be fitted by equation (3.1); we obtain $k = 0.2$, and f of the order of 100 at low temperature (550°C). Both these parameter values seem quite high compared with those typically obtained in metals, where $k \sim 0.01$ and $f \sim 1$ (e.g. [64]). One possible reason for the apparent large values of k and f is the existence of additional recovery processes not included in equation (3.1), notably dislocation climb. Therefore, the estimates based on single crystal data at elevated temperature (figure 3) should be viewed with caution, and we will investigate the behaviour of the system with a wider range of parameter values.

The full model including microcracks requires the use of several additional parameters. The fracture toughness is quite well constrained in many rock-forming minerals [65] and is $K_{\text{Ic}} = 0.2 \text{ MPa m}^{1/2}$ for calcite at room temperature [66,67]. Microcrack spacing L_c can be extracted from crack density observations (e.g. [4,8,21]), which typically report quantities of the order of a few cracks per grain in Carrara marble at high pressure. For simplicity, we will assume that L_c is equal to grain size, which produces the required order of magnitude. By contrast, the quantities like pile-up density ρ_{pu} , pile-up length L and the fraction of dislocations stored in pile-ups ϕ are yet to be constrained by any experimental data or observations. Due to the simplified nature of the model, it is unlikely that direct measurements can be made to identify these parameters with certainty. Here, we have to rely on a general assessment in terms of order of magnitude and make elementary predictions. Following Nicolas *et al.* [25], we will use $\rho_{\text{pu}} = 10^8 \text{ m}^{-2}$, $L = d$ (grain size) and ϕ up to 1. The nominal crack spacing L_c , taken equal to the grain size, is consistent with the assumption that cracks nucleate at pile-ups. One final parameter required by the model is related to the level of backstress: as noted earlier, the expression (2.4) is the backstress due to an isolated dislocation pile-up, and the average backstress in the aggregate is most likely much smaller than this value. To reflect this fact, we introduce an *ad hoc* factor $f_b \ll 1$ that multiplies σ_b and set it to a constant. Table 1 summarizes the parameter values used to model calcite deformation, and table 2 provides the list of symbols used in the model.

Table 1. List of model parameters relevant to calcite aggregates.

parameter	value
Taylor factor, $\alpha' M$	1.34
Burgers vector, b	6.37 Å
shear modulus, G	32 GPa
Poisson's ratio, ν	0.28
forest hardening parameter, k	0.2
dynamic recovery parameter, f	0–200
backstress factor, f_b	0.01
effective grain size, d_{eff}	150 μm
fraction of dislocations in pile-ups, ϕ	0.1–1
pile-up density, ρ_{pu}	10^8 m^{-2}
fracture toughness, K_{Ic}	0.2 MPa/m ^{1/2}
crack angle, θ	$\pi/4$

4. Results

(a) General features

The model predicts a nonlinear strain-hardening behaviour that depends on confining pressure (taken as σ_2 in the model; figure 4). At low pressure, cracks can grow easily and efficiently limit dislocation storage. With increasing pressure, crack growth is limited and more dislocations are stored, leading to significant hardening. A steady-state in terms of dislocation density, crack length and stress can be achieved when the sink terms (due to cracking and dynamic recovery) match the source terms (due to grain size and forest hardening). With the large parameter f inferred from single crystal data, of the order of 100, the steady-state is achieved after around 5% strain.

When cracking is not accounted for, there is no predicted pressure dependency: strain hardening continues until the steady-state $\rho = (k/(bf))^2$ is reached. In practice, at low temperature, this steady-state may correspond to very large dislocation densities, and it is not clear if this situation is realistic in the absence of dislocation climb processes.

The model output is strongly influenced by all the newly introduced parameters: with increasing ϕ , microcrack growth initiates at lower strain and produces an earlier stabilization of the dislocation density (figure 5a). With increasing f_b , the strain hardening rate increases markedly (figure 5b). Variations in k and f do not change the steady-state behaviour if they remain in the same proportions; however, decreasing both k and f reduces the dislocation storage rate and thus delays the initiation of microcracking and limits microcrack growth (figure 5c).

(b) Comparison with data

The model predicts, almost by design, that strain-hardening rates decrease with increasing strain, and increase with confining pressure. Hardening rates predicted by the model are of a similar order of magnitude as and follow similar trends to those observed experimentally in Carrara marble by Rybacki *et al.* [5] (figure 6), but are not quantitatively accurate. With the parameter values of table 1, and only changing the recovery parameter f at different temperatures, the model tends to overpredict the reduction in hardening rate with increasing strain. In

Table 2. List of symbols.

name	symbol	units
resolved shear stress	τ	Pa
lattice friction	τ_0	Pa
Taylor factor	M	—
dislocation interaction strength	α, α'	—
Burgers vector	b	m
dislocation density	ρ	m^{-2}
applied stress	σ	Pa
yield stress	σ_0	Pa
additional backstress	σ_b	Pa
shear modulus	G	Pa
Poisson ratio	ν	—
number of dislocation in pile-ups	n_p	—
pile-up length	L	m
fraction of total dislocation density stored in pile-ups	ϕ	—
pile-up density	ρ_{pu}	m^{-2}
shear strain	ϵ	—
dislocation mean-free path	λ	m
dynamic recovery factor	f	—
forest hardening coefficient	k	—
grain size	d	m
fracture toughness	K_{Ic}	$\text{Pa m}^{1/2}$
shear stress driving dislocation pile-up	τ_{eff}	Pa
critical number of dislocations in pile-up	n_c	—
normal stress on tensile crack	σ_n	Pa
tensile crack length	ℓ	m
pile-up angle from axial load	ξ	—
tensile crack angle from pile-up	θ	—
applied axial stress	σ_1	Pa
applied confining stress	σ_3	Pa
average crack spacing	L_c	m
twin spacing	t	m
effective grain/twin spacing	d_{eff}	m

the absence of cracking, the characteristic strain at which hardening drops is of the order of $1/f$, and reduces further if cracking occurs. Decreasing the parameter f does not significantly improve the fit to the data, because the resulting increase in dislocation storage is balanced by a decrease due to additional cracking.

Further comparison with experimental data in terms of predicted hardening rates at different grain sizes [21] shows some shortcomings in the modelling approach (figure 7). Both strength and hardening rate measured at 5% strain decrease with increasing grain size at grain

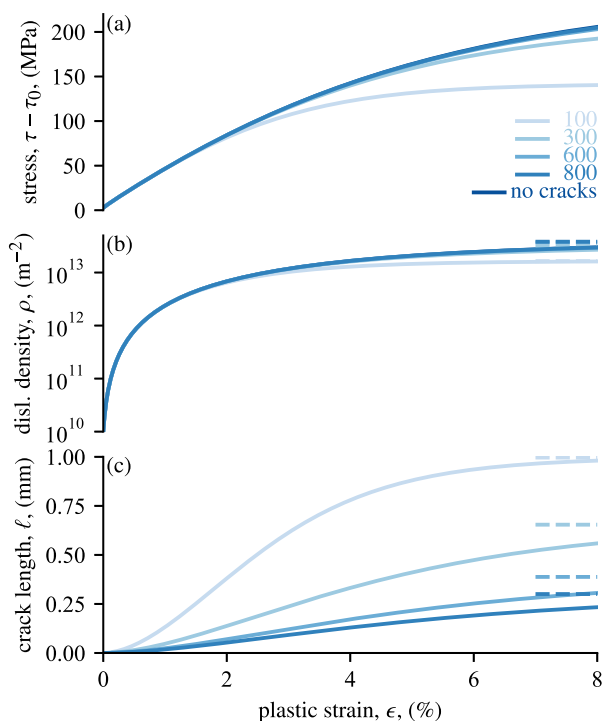


Figure 4. Model prediction for stress variation, dislocation density and tensile crack length with increasing plastic strain for a range of confining pressures (values given in MPa in panel (a)). We set $f_b = 0.001$, $\phi = 0.5$ and $f = 50$. Other parameter values are given in table 1. Dashed lines in panels (b) and (c) indicate steady-state solutions.

sizes above around 100 μm , which is broadly consistent with available data in calcite. However, the modelled behaviour at smaller grain sizes shows a decrease in strength and hardening rate that is at odds with experimental data. This discrepancy arises due to the strong dependency of crack growth on pile-up length L , which is taken here equal to the grain size: with decreasing grain size, fewer dislocations are required to initiate cracks (2.10), and the dislocation sink mechanism is very effective ((2.15), with $L_c = d$), which together limit hardening rates. It is clear that this mechanism is not correct: experimental results show a clear increase in strength and hardening with decreasing grain size. Unfortunately, experimental observations of crack densities in the semi-brittle regime in fine-grained calcite rocks are scarce, and it is not currently possible to directly probe if cracking is indeed more prevalent in these rocks compared with coarser grained materials. Recent ultrasonic results by Harbord *et al.* [21] suggest that Solnhofen limestone (grain size of the order of 10 μm) undergoes more microcracking than Carrara marble (grain size of the order of 100 μm) during deformation at high pressure, low temperature, as evidenced by a more marked decrease in wave velocity with increasing strain. Nevertheless, the mechanical data clearly show that fine-grained rocks are stronger and harden at least as much as coarse-grained materials: the effect of cracks is thus more limited than predicted by the model.

A number of possibilities exist to solve the discrepancy, such as: (i) an increase in toughness with decreasing grain size, e.g. due to bridging or cracks stopping at grain boundaries; or (ii) a significant decrease in the number of dislocations stored in pile-ups when the grain size is small. Both these options would require changing one or several model parameters as a function of grain size, so the model could be modified to produce the required qualitative behaviour. The appropriate modifications would however require further work and independ-

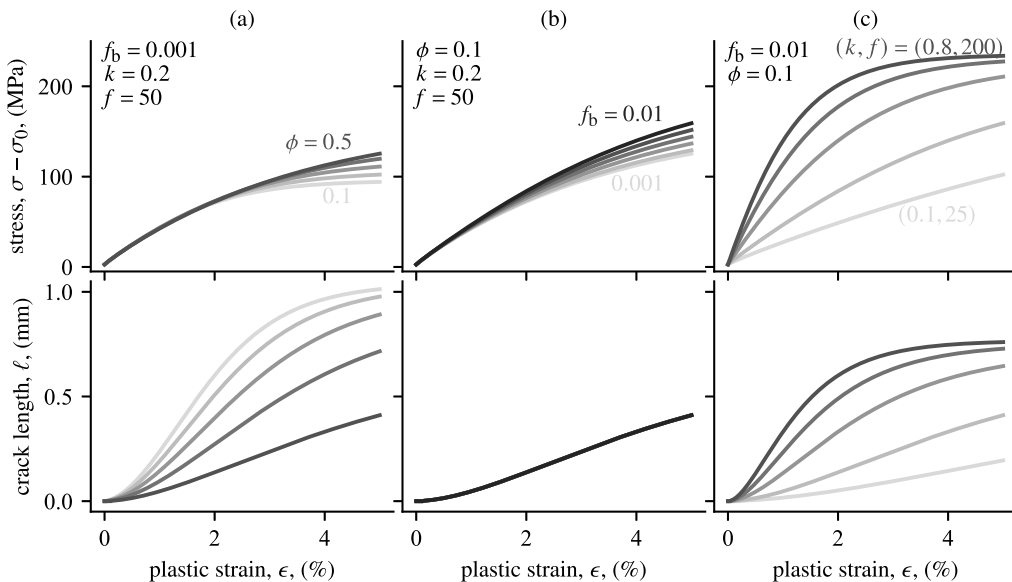


Figure 5. Impact of parameters on model predictions for stress (top) and crack length evolution (bottom). (a) Effect of variations in ϕ from 0.1 to 0.5. (b) Effect of variations in f_b from 0.001 to 0.1. (c) Effect of variations in k and f , kept in the same proportions ($k/f = 0.004$), with k ranging from 0.1 to 0.8.

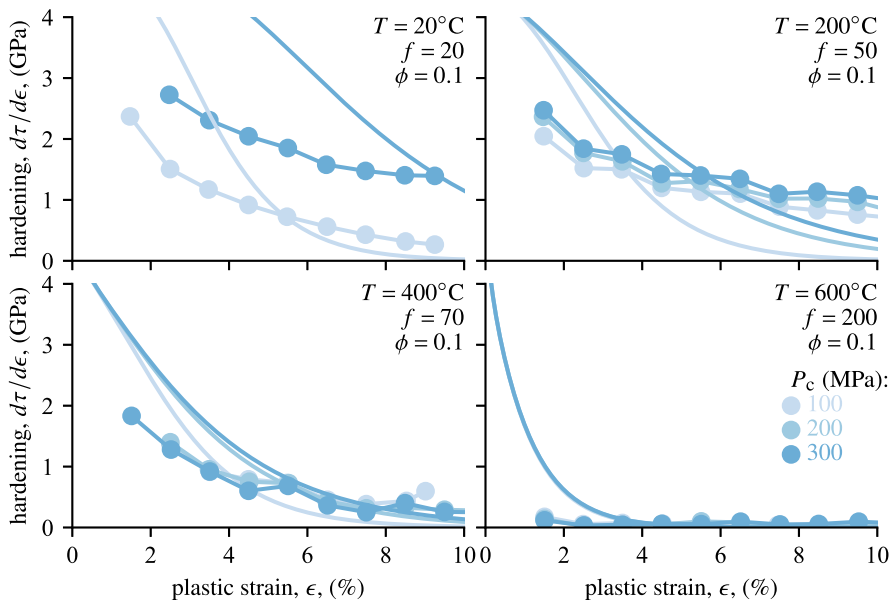


Figure 6. Predicted hardening rates (solid lines) as function of strain in Carrara marble, and comparison with data (circles) from Rybacki *et al.* [5]. Increasing temperature can be simulated by increasing the recovery parameter f .

ent experimental data, notably in terms of crack density, toughness and more generally dislocation density.

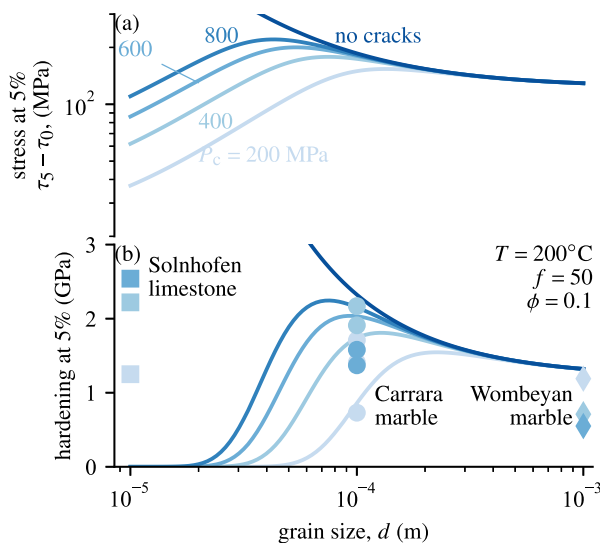


Figure 7. Modelled stress change (a) and hardening rate (b) at 5% strain as functions of grain size, and comparison with available experimental data [21].

5. Discussion and conclusions

(a) Limitations

The comparison of model predictions with available laboratory data on calcite highlights several important limitations of the modelling approach. First, the quantitative agreement in terms of hardening as a function of strain at different pressures is not great (figure 6). Second, the grain size effect is not correctly predicted in fine-grained materials.

We should keep in mind that the model has been kept as simple and elementary as possible, so that the role of microcracks (initiating and growing from pile-ups, and sinks to mobile dislocations) could be investigated without any further complexity. Even in this simple framework, the model contains many parameters that are not well constrained by independent datasets. Several parameters are difficult to observe directly and are not material constants, such as the pile-up density, backstress factor and the fraction of dislocations stored in pile-ups. Variations in these parameters are not expected to change the qualitative nature of the results, but only impact quantitatively the effectiveness of crack generation and its role in limiting dislocation density (and thus hardening). The factors in the KME equation are better constrained, since we can rely on independent data on single crystals. However, the constraints are limited, since the forest hardening parameter k and dynamic recovery parameter f had to be constrained by deformation and dislocation density data obtained at temperatures higher than those directly relevant to semi-brittle flow. A considerable simplification used here was to consider that a fixed proportion of stored dislocations form pile-ups: this assumption is likely too restrictive. Furthermore, while anecdotal evidence exists for a Bauschinger effect in rocks deformed in the semi-brittle regime, the level of backstress remains poorly known. It was measured recently in olivine at room temperature and 1250°C by Hansen *et al.* [9] and Hansen *et al.* [41], respectively, but it is not known in calcite marble and more systematic data are needed in many rock types.

Despite the wide range of possible parameter values allowed in the absence of firm independent measurements, it is difficult to make the model fit all observations, especially the grain size dependence. More complexity is clearly required, with more detailed physics of the microcrack growth mechanisms. Possibilities of extension include toughening mechanisms due to cracks encountering grain boundaries and crack-tip shielding by dislocations ([53], Chap. 7).

Dislocations ‘dragged’ at crack tips have been observed in olivine single crystals [68]. Unfortunately, these processes are hard to quantify in rock-forming minerals, and detailed modelling attempts are perhaps premature at this stage.

(b) Other deformation mechanisms and models

We assumed here that all the shear strain was due to dislocation motion. This is an end-member scenario that allowed us to capture the specific feedback of cracking on plastic flow. In nature, more deformation mechanisms coexist in the semi-brittle regime. Microcracking itself produces additional strain; with purely vertical cracks as assumed here, the additional strain is only in the radial direction and not in the axial direction, and microcracking only contributes to dilational volumetric strain. Twinning contributes to shear strain and could be included in the model by considering the volume fraction of twins and its evolution with deformation (e.g. [28]). Experimental data in calcite tend to show that twin spacing is not strongly dependent on strain beyond a few per cent axial strain [22,59], so only the early stages of deformation should be impacted by this contribution. As discussed earlier and more extensively in Rybacki *et al.* [5], twinning may lead to additional hardening by reducing dislocation mean-free path: the modelling approach is perfectly suited to include those effects, but more systematic data are needed to fully constrain the appropriate parameter values.

One other mechanism that likely operates in the low pressure regime in parallel to dislocation glide is frictional sliding between neighbouring grains. Frictional slip on pre-existing defects, although not directly documented in semi-brittle microstructures, has been extensively studied in the context of micromechanics of brittle deformation in rocks (e.g. [69], §6.2). It can produce inelastic shear strain, hysteresis in stress–strain behaviour (analogue to backstress effects), and can be the source of tensile microcracks. In the model of Nicolas *et al.* [25], sliding defects and their associated tensile cracks were included in series with other inelastic processes, and no feedback between frictional slip, cracking and dislocation motion was included. The model proposed here is well suited to include separate cracking processes, arising for instance from frictional slip (so-called ‘wing cracks’). This can be done by using a more general internal state variable that represents crack density (instead of our ℓ that was completely determined by dislocation pile-ups) and determine an evolution law for this quantity based on all cracking sources. As stated by Wong [45], the mathematics of tensile cracking from dislocation pile-ups is strictly the same as that from sliding frictional defects, because linear elastic fracture mechanics applies regardless of the source of initial slip and stress concentration. It is thus possible to consider other microcracking sources within the same framework.

In our model, we considered open cracks as dislocation sinks. While it is a plausible hypothesis when we think of dislocations disappearing (and generating steps) at free surfaces, the situation is more complicated if we consider the role of crack tips. In ductile materials, the large stress concentration at elastic crack tips is relaxed by plastic processes, so that crack tips may be sources of dislocations within grains (as evidenced in olivine and calcite, see for instance [4,68]). It is not clear at this stage how crack tip dislocations can be accounted for in a model: it is possible that those dislocations locally contribute to an increase in toughness, but they may also contribute more generally to stored dislocations.

(c) Outlook

In an early micromechanical model of the brittle-plastic transition in rocks, [23] considered plasticity to be induced by primarily brittle or frictional processes. This was also the case in the approach of Renshaw & Schulson [24], who used the concept of plastic zones ahead of tensile cracks to determine the nature of fracture growth. In other words, those models considered the effects of plastic flow in a primarily brittle material. Recent work revisiting the approach of Horii & Nemat-Nasser [23] shows that the contribution of plasticity dominates the overall

deformation at large strain [17], which highlights the importance of using a sufficiently realistic plastic flow model. Here, we approached the problem of semi-brittle flow by considering the effect of cracks in a primarily plastic material, where dislocations are the main carrier of deformation as well as the potential source of tensile cracks.

This approach appears quite promising: The proposed model is capable of reproducing the pressure dependency of strength and hardening rate that is commonly observed in the semi-brittle regime. The mechanism suggested here is that dislocation accumulation leads to microcracking, which in turns leads to a weakening effect by allowing mobile dislocations to escape the crystal lattice when they reach the free surfaces of the cracks.

The model is evidently oversimplified and cannot yet reproduce all experimental observations without further parameter adjustments or added complexity. Nevertheless, the KME approach is shown here to be a viable starting point to better understand the semi-brittle regime. Extensions to time-dependent aspects including multiple recovery mechanisms have been shown to be very successful in modelling grain size sensitive plastic flow of olivine [34,43]. Coupling with twinning processes is also feasible to model calcite marbles [5,21].

The source of microcracks was assumed to be dislocation pile-ups, which followed previous work [25,45]. In this approach, the number of crack nuclei per unit volume is equal to the pile-up density, and the only evolving quantity is the average crack length. However, in the absence of direct and systematic microstructural observations, this choice is likely overly restrictive. A more general idea could be to include the effect of microcracks using one or more crack density parameters (e.g. crack density tensors as in linear elasticity [70]) and make those parameters evolve in a more phenomenological manner, based on a microcrack nucleation and/or growth rate that depends for instance on accumulated plastic strain or other macroscopic quantities. Such an approach might be more flexible, at the cost of fitting *ad hoc* phenomenological quantities that could be hard to extrapolate over geological scales.

In any case, to go beyond basic comparisons of macroscopic stress–strain behaviour, detailed microstructural observations in experimentally deformed samples are required. A rigorous test of the KME approach and its proposed extensions requires systematic, quantitative dislocation density data, together with twin volume, crack density and stress–strain behaviour in rocks deformed in the semi-brittle regime. Perhaps the most critical task is to measure average dislocation density in deformed samples, which is labour-intensive and challenging when dislocations cannot be easily decorated by chemical processes [71]. Modern microscopy techniques such as high-resolution electron backscatter diffraction could be used to determine average densities of geometrically necessary dislocations (e.g. [11,72,73]).

Data accessibility. This article has no additional data.

Declaration of AI use. I have not used AI-assisted technologies in creating this article.

Authors' contributions. N.B.: conceptualization, data curation, formal analysis, funding acquisition, investigation, methodology, project administration, resources, software, supervision, validation, visualization, writing—original draft, writing—review and editing.

Conflict of interest declaration. I declare I have no competing interests.

Funding. Financial support from the European Research Council under the European Union's Horizon 2020 research and innovation programme (project Rock-DEaF, grant agreement #804685 to N.B.), from the UK Natural Environment Research Council (grant NE/M016471/1) and from the Leverhulme Trust (Philip Leverhulme Prize) is gratefully acknowledged.

Acknowledgements. This work has benefitted from many discussions with Thomas Breithaupt, Brian Evans, Lars Hansen, Chris Harbord, Tongzhang Qu, Jörg Renner, Erik Rybacki, Chris Spiers and David Wallis. In particular, Lars Hansen provided key comments on an early version of the manuscript. Critical comments by three reviewers helped improve the manuscript.

References

1. Evans B, Fredrich JT, Wong TF. 1990 The brittle-ductile transition in rocks: Recent experimental and theoretical progress. In *The brittle-ductile transition in rocks: the heard volume*. *Geophys. Monogr. Ser* (eds AG Duba, WB Durham, JW Handin, HF Wang), pp. 1–20. Washington, DC: American Geophysical Union. (doi:10.1029/GM056p0001)
2. Kohlstedt DL, Evans B, Mackwell SJ. 1995 Strength of the lithosphere: Constraints imposed by laboratory experiments. *J. Geophys. Res.* **100**, 17587–17602. (doi:10.1029/95JB01460)
3. Evans B, Kohlstedt DL. 2013 Rheology of Rocks. In *Rock physics and phase relations: a handbook of physical constants* (ed. TJ Ahrens), pp. 148–165. Washington, DC: American Geophysical Union.
4. Fredrich JT, Evans B, Wong T. 1989 Micromechanics of the brittle to plastic transition in Carrara marble. *J. Geophys. Res.* **94**, 4129–4145. (doi:10.1029/jb094ib04p04129)
5. Rybacki E, Niu L, Evans B. 2021 Semi-brittle deformation of Carrara marble: hardening and twinning induced plasticity. *J. Geophys. Res.* **126**, B022573. (doi:10.1029/2021jb022573)
6. Hirth G, Tullis J. 1994 The brittle-plastic transition in experimentally deformed quartz aggregates. *J. Geophys. Res.* **99**, 11731–11747. (doi:10.1029/93JB02873)
7. Druiventak A, Trepmann CA, Renner J, Hanke K. 2011 Low-temperature plasticity of olivine during high stress deformation of peridotite at lithospheric conditions — An experimental study. *Earth Planet. Sci. Lett.* **311**, 199–211. (doi:10.1016/j.epsl.2011.09.022)
8. O’Ghaffari H, Peč M, Mittal T, Mok U, Chang H, Evans B. 2023 Microscopic defect dynamics during a brittle-to-ductile transition. *Proc. Natl Acad. Sci. USA* **120**, e2305667. (doi:10.1073/pnas.2305667120)
9. Hansen LN, Kumamoto KM, Thom CA, Wallis D, Durham WB, Goldsby DL, Breithaupt T, Meyers CD, Kohlstedt DL. 2019 Low-temperature plasticity in olivine: Grain size, strain hardening, and the strength of the lithosphere. *J. Geophys. Res.* **124**, 5427–5449. (doi:10.1029/2018jb016736)
10. Meyer GG, Brantut N, Mitchell TM, Meredith PG. 2019 Fault reactivation and strain partitioning across the brittle-ductile transition. *Geology* **47**, 1127–1130. (doi:10.1130/g46516.1)
11. Wallis D *et al.* 2020 Dislocation interactions during low-temperature plasticity of olivine and their impact on the evolution of lithospheric strength. *Earth Planet. Sci. Lett.* **543**, 116349. (doi:10.1016/j.epsl.2020.116349)
12. Mecking H, Kocks UF. 1981 Kinetics of flow and strain-hardening. *Acta Metall.* **29**, 1865–1875. (doi:10.1016/0001-6160(81)90112-7)
13. Kocks UF, Mecking H. 2003 Physics and phenomenology of strain hardening: the FCC case. *Prog. Mater. Sci.* **48**, 171–273. (doi:10.1016/s0079-6425(02)00003-8)
14. Lawn BR, Marshall DB. 1998 Nonlinear stress-strain curves for solids containing closed cracks with friction. *J. Mech. Phys. Solids* **46**, 85–113. (doi:10.1016/s0022-5096(97)00036-7)
15. David EC, Brantut N, Hirth G. 2020 Sliding crack model for nonlinearity and hysteresis in the triaxial stress-strain curve of rock, and application to antigorite deformation. *J. Geophys. Res.* **125**, B018970. (doi:10.1029/2019jb018970)
16. Taylor GI. 1934 The mechanism of plastic deformation of crystals. part i.—theoretical. *Proc. R. Soc. Lond.* **145**, 362–387.
17. Liu D, Brantut N. 2023 Micromechanical controls on the brittle-plastic transition in rocks. *Geophys. J. Int.* **234**, 562–584. (doi:10.1093/gji/ggad065)
18. Brantut N, Petit L. 2022 Micromechanics of rock damage and its recovery in cyclic loading conditions. *Geophys. J. Int.* **233**, 145–161. (doi:10.1093/gji/ggac447)
19. Mitchell TE, Hirth JP. 1991 The shape, configuration and stress field of twins and martensite plates. *Acta Metall. Mater.* **39**, 1711–1717. (doi:10.1016/0956-7151(91)90260-8)
20. Edmond JM, Paterson MS. 1972 Volume changes during the deformation of rocks at high pressures. *Int. J. Rock Mech. Min. Sci.* **9**, 161–182.
21. Harbord C, Brantut N, Wallis D. 2023 Grain-size effects during semi-brittle flow of calcite rocks. *J. Geophys. Res.* **128**, B026458. (doi:10.1029/2023jb026458)

22. Rowe KJ, Rutter EH. 1990 Palaeostress estimation using calcite twinning: experimental calibration and application to nature. *J. Struct. Geol.* **12**, 1–17. (doi:10.1016/0191-8141(90)90044-y)
23. Horii H, Nemat-Nasser S. 1986 Failure in compression: Splitting, faulting and brittle-ductile transition. *Philos. Trans. R. Soc. Lond.* **319**, 337–374.
24. Renshaw CE, Schulson EM. 2001 Universal behaviour in compressive failure of brittle materials. *Nature* **412**, 897–900. (doi:10.1038/35091045)
25. Nicolas A, Fortin J, Regnet JB, Verberne BA, Plümper O, Dimanov A, Spiers CJ, Guéguen Y. 2017 Brittle and semibrittle creep of Tavel limestone deformed at room temperature. *J. Geophys. Res.* **122**, 4436–4459. (doi:10.1002/2016jb013557)
26. Devincere B, Hoc T, Kubin L. 2008 Dislocation mean free paths and strain hardening of crystals. *Science* **320**, 1745–1748. (doi:10.1126/science.1156101)
27. Estrin Y, Mecking H. 1984 A unified phenomenological description of work hardening and creep based on one-parameter models. *Acta Metall.* **32**, 57–70. (doi:10.1016/0001-6160(84)90202-5)
28. Bouaziz O, Allain S, Scott C. 2008 Effect of grain and twin boundaries on the hardening mechanisms of twinning-induced plasticity steels. *Scr. Mater.* **58**, 484–487.
29. De Cooman BC, Estrin Y, Kim SK. 2018 Twinning-induced plasticity (TWIP) steels. *Acta Mater.* **142**, 283–362. (doi:10.1016/j.actamat.2017.06.046)
30. Sauzay M, Kubin LP. 2011 Scaling laws for dislocation microstructures in monotonic and cyclic deformation of fcc metals. *Prog. Mater. Sci.* **56**, 725–784. (doi:10.1016/j.pmatsci.2011.01.006)
31. Kohlstedt DL, Weathers MS. 1980 Deformation-induced microstructures, paleopiezometers, and differential stresses in deeply eroded fault zones. *J. Geophys. Res.* **85**, 6269–6285. (doi:10.1029/jb085ib11p06269)
32. de Bresser JHP. 1996 Steady state dislocation densities in experimentally deformed calcite materials: Single crystals versus polycrystals. *J. Geophys. Res.* **101**, 22189–22201. (doi:10.1029/96JB01759)
33. Thom CA, Hansen LN, Breithaupt T, Goldsby DL, Kumamoto KM. 2022 Backstresses in geologic materials quantified by nanoindentation load-drop experiments. *Philos. Mag.* **102**, 1974–1988.
34. Breithaupt T, Katz RF, Hansen LN, Kumamoto KM. 2023 Dislocation theory of steady and transient creep of crystalline solids: Predictions for olivine. *Proc. Natl Acad. Sci. USA* **120**, e2203448120. (doi:10.1073/pnas.2203448120)
35. Kohlstedt DL, Goetze C. 1974 Low-stress high-temperature creep in olivine single crystals. *J. Geophys. Res.* **79**, 2045–2051. (doi:10.1029/jb079i014p02045)
36. Durham WB, Goetze C, Blake B. 1977 Plastic flow of oriented single crystals of olivine: 2. Observations and interpretations of the dislocation structures. *J. Geophys. Res.* **82**, 5755–5770. (doi:10.1029/jb082i036p05755)
37. Bai Q, Kohlstedt DL. 1992 High-temperature creep of olivine single crystals, 2. dislocation structures. *Tectonophysics* **206**, 1–29. (doi:10.1016/0040-1951(92)90365-d)
38. Durinck J, Devincere B, Kubin L, Cordier P. 2007 Modeling the plastic deformation of olivine by dislocation dynamics simulations. *Am. Mineral.* **92**, 1346–1357.
39. Sinclair CW, Poole WJ, Brechet Y. 2006 A model for the grain size dependent work hardening of copper. *Scr. Mater.* **55**, 739–742.
40. Holcomb DJ. 1981 Memory, relaxation, and microfracturing in dilatant rock. *J. Geophys. Res.* **86**, 6235–6248. (doi:10.1029/JB086iB07p06235)
41. Hansen LN, Wallis D, Breithaupt T, Thom CA, Kempton I. 2021 Dislocation creep of olivine: Backstress evolution controls transient creep at high temperatures. *J. Geophys. Res.* **126**, B021325. (doi:10.1029/2020jb021325)
42. Eshelby JD, Frank FC, Nabarro FRN. 1951 The equilibrium of linear arrays of dislocations. *Philos. Mag.* **42**, 351–364.
43. Breithaupt T. 2021 Modelling elements of microstructure in olivine. PhD thesis, University of Oxford, UK.
44. Olsson WA, Peng SS. 1976 Microcrack nucleation in marble. *Int. J. Rock Mech. Min. Sci. & Geomech. Abstr.* **13**, 53–59. (doi:10.1016/0148-9062(76)90704-X)

45. Wong T. 1990 A note on the propagation behavior of a crack nucleated by a dislocation pileup. *J. Geophys. Res.* **95**, 8639–8646. (doi:10.1029/jb095ib06p08639)
46. Stroh AN. 1954 The formation of cracks as a result of plastic flow. *Proc. R. Soc. Lond.* **223**, 404–414.
47. Stroh AN. 1958 The cleavage of metal single crystals. *Philos. Mag.* **3**, 597–606.
48. Francois D, Wilshaw TR. 1968 The effect of hydrostatic pressure on the cleavage fracture of polycrystalline materials. *J. Appl. Phys.* **39**, 4170–4177. (doi:10.1063/1.1656943)
49. Darot M, Gueguen Y, Benchemam Z, Gaboriaud R. 1985 Ductile-brittle transition investigated by micro-indentation: results for quartz and olivine. *Phys Earth Planet Int* **40**, 180–186.
50. Wallis D, Hansen LN, Britton TB, Wilkinson AJ. 2017 Dislocation interactions in olivine revealed by HR-EBSD. *J. Geophys. Res.* **122**, 7659–7678. (doi:10.1002/2017jb014513)
51. Sayers CM, Kachanov M. 1995 Microcrack-induced elastic wave anisotropy of brittle rocks. *J. Geophys. Res.* **100**, 4149–4156. (doi:10.1029/94jb03134)
52. Basista M, Gross D. 1998 The sliding crack model of brittle deformation: An internal variable approach. *Int. J. Solids Struct.* **35**, 487–509. (doi:10.1016/s0020-7683(97)00031-0)
53. Lawn BR. 1993 *Fracture of brittle solids*, 2nd edn. Cambridge, UK: Cambridge University Press.
54. Caillard D, Martin JL. 2003 *Thermally activated mechanisms in crystal plasticity*. Oxford, UK: Pergamon. (Pergamon Materials Series).
55. Barber DJ, Wenk HR. 1979 Deformation twinning in calcite, dolomite, and other rhombohedral carbonates. *Phys. Chem. Miner.* **5**, 141–165. (doi:10.1007/bf00307550)
56. Spiers CJ. 1979 Fabric development in calcite polycrystals deformed at 400c. *Bull. De Minéralogie* **102**, 282–289.
57. Quintanilla-Terminel A, Evans B. 2016 Heterogeneity of inelastic strain during creep of Carrara marble: Microscale strain measurement technique. *J. Geophys. Res.* **121**, 5736–5760. (doi:10.1002/2016jb012970)
58. Bayerschen E, McBride AT, Reddy BD, Böhlke T. 2016 Review on slip transmission criteria in experiments and crystal plasticity models. *J. Mater. Sci.* **51**, 2243–2258. (doi:10.1007/s10853-015-9553-4)
59. Rybacki E, Evans B, Janssen C, Wirth R, Dresen G. 2013 Influence of stress, temperature, and strain on calcite twins constrained by deformation experiments. *Tectonophysics* **601**, 20–36. (doi:10.1016/j.tecto.2013.04.021)
60. Goetze C, Kohlstedt DL. 1977 The dislocation structure of experimentally deformed marble. *Contrib. Mineral. Petrol.* **59**, 293–306. (doi:10.1007/bf00374558)
61. Briegel U, Goetze C. 1978 Estimates of differential stress recorded in the dislocation structure of Lochseiten Limestone (Switzerland). *Tectonophysics* **48**, 61–76. (doi:10.1016/0040-1951(78)90086-0)
62. Schmid SM, Paterson MS, Boland JN. 1980 High temperature flow and dynamic recrystallization in carrara marble. *Tectonophysics* **65**, 245–280. (doi:10.1016/0040-1951(80)90077-3)
63. Schmid SM, Boland JN, Paterson MS. 1977 Superplastic flow in finegrained limestone. *Tectonophysics* **43**, 257–291. (doi:10.1016/0040-1951(77)90120-2)
64. Bouaziz O, Guelton N. 2001 Modelling of TWIP effect on work-hardening. *Mater. Sci. Eng.* **319–321**, 246–249. (doi:10.1016/s0921-5093(00)02019-0)
65. Atkinson BK. 1984 Subcritical crack growth in geological materials. *J. Geophys. Res.* **89**, 4077–4114. (doi:10.1029/jb089ib06p04077)
66. Santhanam AT, Gupta YP. 1968 Cleavage surface energy of calcite. *Int. J. Rock Mech. Min. Sci.* **5**, 253–259.
67. Atkinson BK, Avdis V. 1980 Fracture mechanics parameters of some rock-forming minerals determined using an indentation technique. *Int. J. Rock Mech. Min. Sci. Geomech. Abstr.* **17**, 383–386. (doi:10.1016/0148-9062(80)90523-9)
68. Gaboriaud RJ, Darot M, Gueguen Y, Woïgard J. 1981 Dislocations in olivine indented at low temperatures. *Phys. Chem. Miner.* **7**, 100–104. (doi:10.1007/bf00309460)
69. Paterson MS, Wong TF. 2005 *Experimental Rock Deformation – The Brittle Field*, 2nd edn. Berlin, Heidelberg, Germany: Springer-Verlag.

70. Kachanov M. 1993 Elastic Solids with Many Cracks and Related Problems. In *Advances in applied mechanics* (eds JW Hutchinson, TY Wu), pp. 259–445, vol. 30. Academic Press.
71. de Bresser JHP. 1991 Intracrystalline deformation of calcite. PhD thesis, Utrecht University, the Netherlands.
72. Jiang J, Britton TB, Wilkinson AJ. 2013 Evolution of dislocation density distributions in copper during tensile deformation. *Acta Mater.* **61**, 7227–7239. (doi:10.1016/j.actamat.2013.08.027)
73. Wallis D, Hansen LN, Britton TB, Wilkinson AJ. 2019 High-angular resolution *electron* backscatter diffraction as a new tool for mapping lattice distortion in geological minerals. *J. Geophys. Res.* **124**, 6337–6358. (doi:10.1029/2019jb017867)